

# The CLYC-6 and CLYC-7 response to $\gamma$ -rays, fast and thermal neutrons

A. Giaz<sup>a</sup>, L. Pellegrini<sup>a</sup>, F. Camera<sup>a,b,\*\*</sup>, N. Blasi<sup>a</sup>, S. Brambilla<sup>a</sup>, S. Ceruti<sup>a,b</sup>, B. Million<sup>a</sup>, S. Riboldi<sup>a,b</sup>, C. Cazzaniga<sup>c,d</sup>, G. Gorini<sup>c,d</sup>, M. Nocente<sup>c,d</sup>, A. Pietropaolo<sup>e</sup>, M. Pillon<sup>e</sup>, M. Rebai<sup>c</sup>, M. Tardocchi<sup>d</sup>

<sup>a</sup>INFN Milano, Via Celoria 16, 20133 Milano, Italy

<sup>b</sup>Università degli Studi di Milano, Physics Dept., Via Celoria 16, 20133 Milano, Italy

<sup>c</sup>University of Milano Bicocca, Physics Dept., Piazza della Scienza 3, 20126 Milano, Italy

<sup>d</sup>Istituto di Fisica del Plasma, Associazione EURATOM-ENEA-CNR, via Roberto Cozzi 53, 20125 Milano, Italy

<sup>e</sup>Associazione EURATOM-ENEA sulla Fusione ENEA C.R. Frascati, Via E. Fermi, 45, 00044 Frascati, Roma, Italy

**\*\*Corresponding author: franco.camera@mi.infn.it**

## Abstract

The crystal  $\text{Cs}_2\text{LiYCl}_6:\text{Ce}$  (CLYC) is a very interesting scintillator material because of its good energy resolution and its capability to identify  $\gamma$ -rays and fast/thermal neutrons. The crystal  $\text{Cs}_2\text{LiYCl}_6:\text{Ce}$  contains  $^6\text{Li}$  and  $^{35}\text{Cl}$  isotopes, therefore, it is possible to detect thermal neutrons through the reaction  $^6\text{Li}(n,\alpha)t$  while  $^{35}\text{Cl}$  ions allow to measure fast neutrons through the reactions  $^{35}\text{Cl}(n, p)^{35}\text{S}$  and  $^{35}\text{Cl}(n, \alpha)^{32}\text{P}$ . In this work two CLYC 1"x1" crystals were measured: the first crystal, enriched with  $^6\text{Li}$  at 95% (CLYC-6) is ideal for thermal neutron measurements while the second one, enriched with  $^7\text{Li}$  at > 99% (CLYC-7) is suitable for fast neutron measurements. The response of CLYC scintillators was measured with different PMT models: timing or spectroscopic, with borosilicate glass or quartz window. The energy resolution, the neutron- $\gamma$  discrimination and the internal activity are discussed. The capability of CLYC scintillators to discriminate  $\gamma$  rays from neutrons was tested with both thermal and fast neutrons. The thermal neutrons were measured with both detectors, using an AmBe source. The measurements of fast neutrons were performed at the Frascati Neutron Generator facility (Italy) where a deuterium beam was accelerated on a deuterium or on a tritium target, providing neutrons of 2.5 MeV or 14.1 MeV, respectively. The different sensitivity to thermal and fast neutrons of a CLYC-6 and of a CLYC-7 was additionally studied.

## 1. Introduction

In the last fifteen years, the search for high performing scintillators produced several new materials [1]. In particular, Lanthanum Halide [2-8], Elpasolite [9-17],  $\text{SrI}_2:\text{Eu}$  [1,18],  $\text{CeBr}_3$  [1,19-20] and Ceramic scintillators [1,21] show better performances than those of the very well-known  $\text{NaI}:\text{Tl}$ ,  $\text{CsI}:\text{Tl}$ , BGO or  $\text{BaF}_2$  scintillators.

A promising class of scintillators are the Elpasolite, discovered about 10 years ago. The  $\text{Cs}_2\text{LiYCl}_6:\text{Ce}$  (CLYC),  $\text{Cs}_2\text{LiLaCl}_6:\text{Ce}$  (CLLC) and  $\text{Cs}_2\text{LiLaCl}_6:\text{Ce}$  (CLLB) scintillators belong to this class. They are characterized by a good energy and time resolution, high linearity, especially at low energy. In particular the CLYC scintillators are characterized by a light yield of  $\sim 20$  ph/keV, a density of  $3.3$  g/cm<sup>3</sup> and an energy resolution of less than 5 % at 662 keV. They can identify and measure  $\gamma$  rays and neutrons at the same time via pulse shape discrimination (PSD)[9-17,22-27].

The sensitivity to thermal neutrons is given by the well known reaction  $^6\text{Li} + n = ^3\text{H} + \alpha$  which has a cross section of 940 barns [9-12]. The emitted tritium ( $^3\text{H}$ ) and the  $\alpha$  particles deposit approximately 3.2 MeVee (MeV electron equivalent). The sensitivity of CLYC to fast neutrons, instead, was found to be given by the reactions on  $^{35}\text{Cl}$  ( $^{35}\text{Cl} + n = ^{35}\text{S} + p$  and  $^{35}\text{Cl} + n = ^{32}\text{P} + \alpha$ ), which have cross sections of the order of 100-300 mb [13-16,22-24]. In addition the energy of the outgoing proton and  $\alpha$  particle scales linearly with the kinetic energy of the incident fast neutron

1 [13,15,24]. Therefore, the energy of the incident neutron can be directly deduced from the amplitude of the pulse  
2 generated by the detector. This unique capability makes CLYC a very promising scintillator for both  $\gamma$  and neutron  
3 spectroscopy in base research and application.

4 Since the capability of CLYC to detect thermal neutrons is provided by  ${}^6\text{Li}$ , the selection of  ${}^6\text{Li}$  or  ${}^7\text{Li}$  enrichment  
5 allows to control the sensitivity of a CLYC scintillator to thermal neutrons. In particular, an enrichment in  ${}^6\text{Li}$  (CLYC-  
6 6) increases the sensitivity to thermal neutrons while an enrichment in  ${}^7\text{Li}$  (CLYC-7) suppresses the sensitivity to  
7 thermal neutrons allowing a better detection of fast neutrons.

8 It has been shown that the CLYC emission light spectrum is characterized by fast and slow components [16]. The  
9 fast component is predominantly induced by  $\gamma$ -rays and it is in the UV part of the spectrum (approximately 220-320  
10 nm). It is generally associated to the CVL (Core to Valence Luminescence) scintillation light which could be partially  
11 or totally reabsorbed and re-emitted by Ce dopant. It has been shown [16] that the intensity of CVL is suppressed as  
12 temperature increases. However the PSD effectiveness in n- $\gamma$  identification is not reduced. The medium and slow  
13 components of the scintillation light are located in the blue region of the light spectrum (approximately 350 nm - 500  
14 nm) and it was shown that they are present in both  $\gamma$ -rays and neutrons induced signals [13-17].

15 There are in literature several studies on the properties of  ${}^6\text{Li}$  enriched detectors (see for example ref [9-17]).  
16 However there are few works on i)  ${}^7\text{Li}$  enriched crystals (almost insensitive to thermal neutrons but good for neutron  
17 spectroscopy) [15], ii) the measurement of CLYC internal radiation [9] and iii) the effects in CLYC performances with  
18 timing PMT or a quartz window PMT. In the first part of this work (section 2) we present the general properties of the  
19 used CLYC-6 (enriched at 95% of  ${}^6\text{Li}$ , as reported in RMD datasheets) and CLYC-7 (with an enrichment of  ${}^7\text{Li}$  larger  
20 than 99%, as reported in RMD datasheets) scintillators [25]. Both detectors show the typical energy resolution already  
21 measured in ref [9-14] but slightly better than the one reported in [15]. Section 2.2 discusses the measurement of  
22 internal radiation in a CLYC-6 crystal showing that it is at least 50 times smaller than that measured in ref [5] for a  
23  $\text{LaBr}_3:\text{Ce}$  of equal size. In the successive section (2.3) the neutron- $\gamma$  discrimination is discussed. We have focused our  
24 attention also on the consequences in the CLYC performances if the UV component of the scintillation light is fully  
25 collected (using a quartz window PMT) or if the extremely fast risetime of the scintillation light (in case of  $\gamma$ -rays) is  
26 preserved in the measurement by using a timing-fast PMT. In fact, the majority of the published works use a  
27 borosilicate window - spectroscopic PMT (usually Hamamatsu 6231-100 / 6233-100 as for example in ref [14] and  
28 [15]). The thermal/fast neutron identification of CLYC-6 and CLYC-7 is described in section 3. Section 3.1 focuses on  
29 thermal neutrons detection pointing out the differences between CLYC-6 and CLYC-7, while section 3.2 describes the  
30 fast neutron detections at 14.1 and 2.5 MeV. The conclusions of the work are described in section 4.

## 31 **2. CLYC properties**

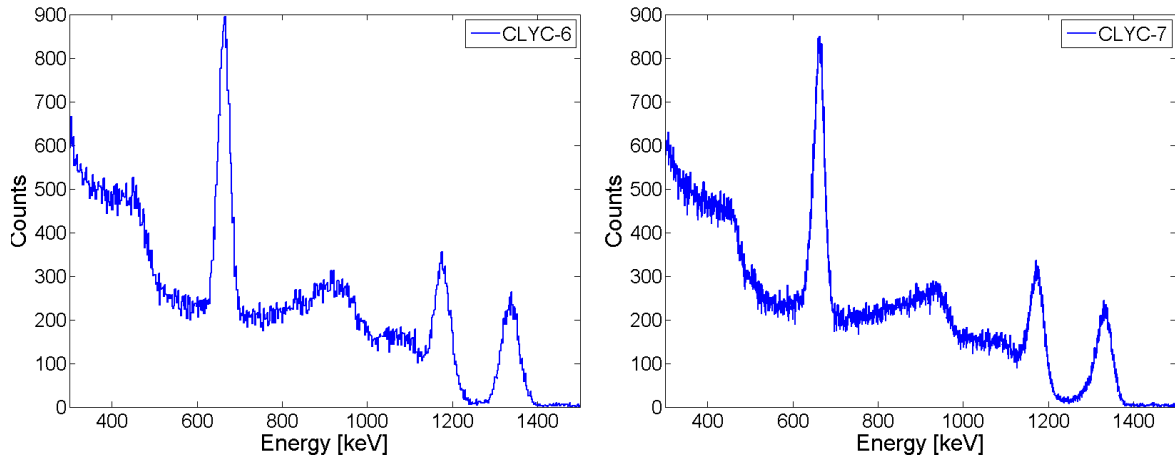
32  
33 Two crystals were used in this work: a CLYC enriched at 95% of  ${}^6\text{Li}$  (CLYC-6) and a CLYC with an enrichment of  
34  ${}^7\text{Li}$  larger than 99% (CLYC-7). Both crystals were produced by RMD and have a cylindrical shape, a diameter of 1''  
35 and a thickness of 1''. For these measurements the CLYC-6 and CLYC-7 scintillators were coupled to a  
36 HAMAMATSU R6231-100mod PMTs and to standard voltage dividers (HAMAMATSU E1198-26 and  
37 HAMAMATSU E1198-27 for CLYC-6 and CLYC-7, respectively).

### 38 **2.1 Energy resolution**

39 CLYC shows a good energy resolution even though the light yield of  $\sim 20$  ph/keV is much smaller than the one of  
40  $\text{NaI:Tl}$ . Indeed, the CLYC crystal has good energy resolution thanks to the excellent linearity [26] for low deposited  
41 energy ( $E < 100$  keV).

42 The  $\gamma$ -ray energy resolution of the two detectors was measured using a MESYTECK MPR-1 charge integrating pre-  
43 amplifier and acquiring the signals with a 12 bit, 600 MHz LeCroy Wave Runner HRO 66Zi oscilloscope. Figure 1  
44 shows the energy spectra of a  ${}^{137}\text{Cs}$  and a  ${}^{60}\text{Co}$  sources measured with CLYC-6 and CLYC-7. The 662 keV peak  
45 produced by the  ${}^{137}\text{Cs}$  source has a FWHM of 32 keV (4.8%) and 30 keV (4.5%), if measured with CLYC-6 and

1 CLYC-7, respectively. The measured energy resolutions are comparable with the RMD datasheet of our two CLYC  
 2 samples, in which they declare an energy resolution of 5% and of 4.6% for CLYC-6 and CLYC-7 respectively. Similar  
 3 energy-resolutions values were found in Ref. [9-14] where different crystals, readout and acquisition systems were  
 4 used.  
 5



6  
 7  
 8 *Figure 1: The energy spectrum of two 1" x 1" CLYC scintillators using a  $^{60}\text{Co}$  and  $^{137}\text{Cs}$  sources. The scintillators were coupled to a*  
 9 *R6231-100mod Hamamatsu PMT with a standard passive voltage divider (HAMAMATSU E1198-26 and E1198-27). The left-panel*  
 10 *shows the spectrum measured with CLYC-6 and the right-panel shows the spectrum measured with CLYC-7.*

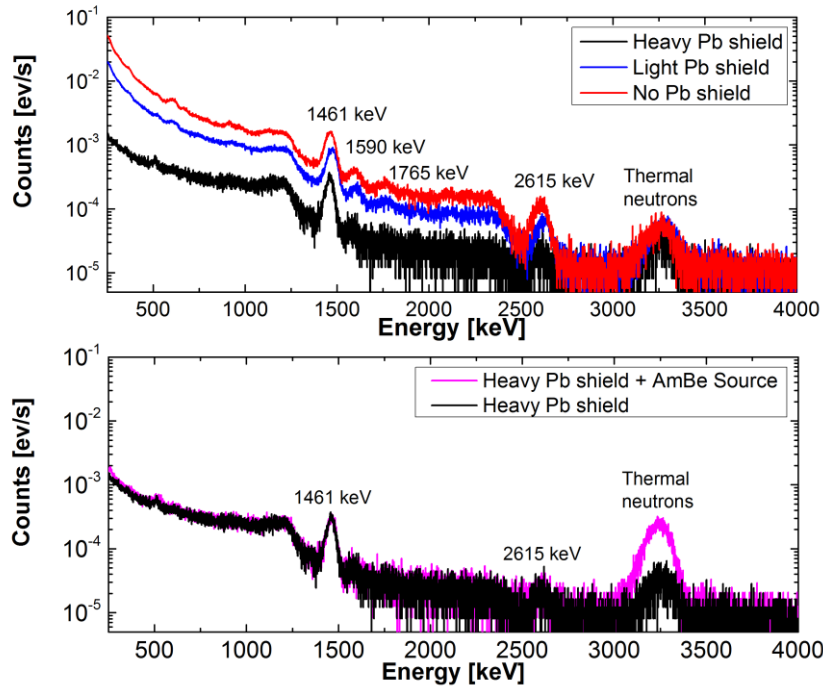
## 11 2.2 Internal activity

12 The internal activity of the CLYC-6 crystal was measured with and without a Pb shield to discriminate between  
 13 intrinsic and natural radiation. It is important to remind that the internal radiation is not affected by the lead shield.

14 In the top panel of figure 2, the spectrum measured with the CLYC-6 without shielding (red line) is compared with  
 15 the spectra measured with 5 cm (blue line) and 10 cm (black line) thick Pb shield. For each measurement, which lasted  
 16 approximately one week, the data are normalized to the live time. It is evident that the intensity of the measured  
 17 radiation decreases as the Pb shield increases (except for the thermal neutron peak around 3.2 MeVee). This suggests  
 18 that all the other peaks in the top panel of figure 3 are from natural background (i.e.  $^{40}\text{K}$ ,  $^{214}\text{Bi}$ ,  $^{208}\text{Tl}$ ).

19 The neutron peak is located at 3.2 MeV and has the same intensity in all spectra as expected since neutrons are not  
 20 affected by the Pb shield. In order to highlight the neutron contribution, an AmBe (placed in a 40 cm polyethylene box)  
 21 thermal neutron source was placed at approximately 2 m from the detector shielded with 10 cm of Pb. The resulting  
 22 spectrum (magenta line) is compared to the one acquired in the same condition but without the neutron source (black  
 23 line) in the bottom panel of figure 2. The two spectra perfectly overlaps, except for the neutron peak which is however  
 24 very weak as few thermal neutrons, escaping from the polyethylene box, interacts in the CLYC-6 detector which was  
 25 located at  $\sim 2$  m of distance. We could not determinate the origin of the extremely small ( $\sim 10^{-4}$  ev/s) thermal neutron  
 26 flux we measure as background.

27 The integral of the spectrum acquired with 10 cm of Pb shield corresponds to a rate of  $0.02$  cts/s/cm<sup>3</sup>. This number  
 28 is approximately 50 times smaller than what measured in reference [5] for a LaBr<sub>3</sub>:Ce of the same volume and can be  
 29 considered the upper limit of the internal radiation in CLYC. Such a low internal radiation makes the CLYC crystal a  
 30 good candidate for low intensity measurements, like, for example, dark matter studies.



1  
2 *Figure 2: (Color on line) Upper panel: the internal and natural radiation spectra acquired using three different type of Pb shields.*  
3 *The red spectrum (the one with more counts) was acquired without any Pb shield, the blue and the black spectra were acquired using*  
4 *5 cm and 10 cm Pb shield, respectively. Bottom panel: the spectra acquired using 10 cm Pb shield with (magenta line) and without*  
5 *(black line) an AmBe thermal neutron source placed approximately 2 m from the detector.*

6

## 7 **2.3 Neutron and $\gamma$ discrimination**

8 The neutron- $\gamma$  discrimination measurements described in this section were performed using CLYC-6. The possibility  
9 to use Pulse Shape Discrimination (PSD) for the identification of the incident radiation is one of the most interesting  
10 features of CLYC. Namely, PSD permits to distinguish  $\gamma$  rays and neutrons because of the differences in the scintillation  
11 decay response. In particular, since the main difference is in the decay time of the scintillation light of the neutron or  $\gamma$   
12 event, we wanted to investigate whether the use of a timing PMT, having a faster rise time with respect to a  
13 spectroscopic PMT, might lead to a better neutron- $\gamma$  identification. Furthermore, we wanted to study the effect of the  
14 CLV component in the signal by comparing PMT's with a borosilicate glass window, which filter about 35% of the  
15 CVL light, to PMT's with a quartz window, which detect completely the CVL component. Since the fast component is  
16 partially in the 250 nm to 350 nm range (CVL), we might expect a different response to a fast signal in the two cases.  
17 Therefore, four different PMT types were tested for neutron- $\gamma$  discrimination, two timing and two spectroscopic ones  
18 with different entrance windows (quartz or borosilicate glass). They are listed in table 1 together with their properties.  
19 The PMT spectral responses are reported in the third column of the table. Note that all the PMTs listed in the table have  
20 the maximum of the quantum efficiency (QE) at 420 ns.

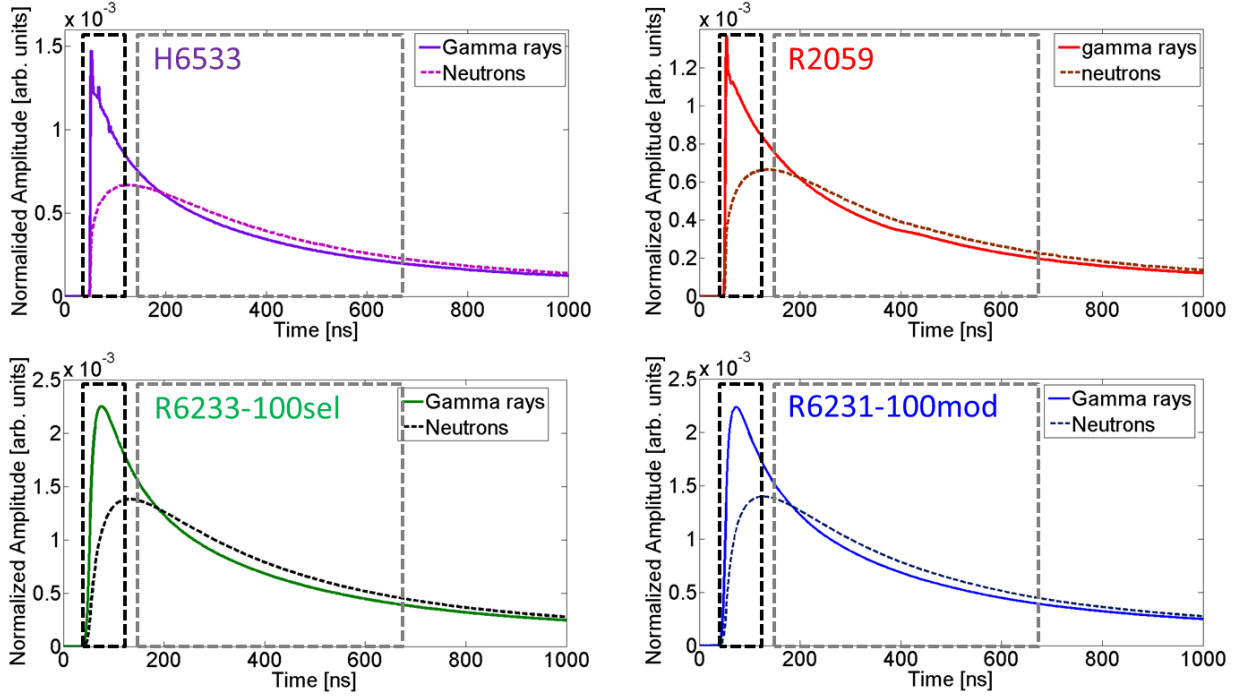
21

PMT	Window material	Spectral response [nm]	Rise Time [ns]	Blue sensitivity index
H6533	Borosilicate glass	300-650	0.7 at 1700 V	10.4
R2059	quartz	160-650	1.3 at 2500 V	11.4
R6233-100sel	Borosilicate glass	300-650	9.5 at 1000 V	15.8
R6231-100mod	quartz	160-650	8.5 at 1000 V	14.0

22

23 *Table 1: The properties of the HAMAMATSU PMTs used in the measurements as listed in the HAMAMATSU datasheet.*  
24 *The window material, the spectral response, the intrinsic rise time and the blue sensitivity are reported in column 2, 3,*  
25 *4, and 5 respectively.*

1 The four PMTs were used to detect  $\gamma$  rays from  $^{137}\text{Cs}$ ,  $^{60}\text{Co}$  and thermal neutrons produced by a AmBe source placed in  
 2 a box of polyethylene. The anode signals were directly sent to the 12 bit, 600 MHz Le Croy waverunner HRO 66Zi  
 3 oscilloscope and digitized. About 10000 pulses were averaged to produce the reference pulses for both  $\gamma$  rays and  
 4 neutrons and are shown in the four panels of figure 3, as indicated in the figure legends. The signal properties measured  
 5 with the different PMTs are reported in Table 2. The timing PMTs, which have a faster intrinsic rise time, show a faster  
 6 component in the  $\gamma$ -ray signals, while the neutron signals maintain a similar rise time. Following the procedure in  
 7 literature (see for example ref. [14]), we set two time windows W1, from the onset of the trace to 80 ns, and W2, from  
 8 110 to 660 ns, as indicated in figure 3 with black and grey dashed boxes, respectively.



10  
11

12 **Figure 3** (color on line): Comparison between a signal produced by a  $\gamma$  ray and by a neutron using the four different PMTs of table  
 13 1. Top-left panel: the used PMT was H6533 that is a timing PMT with a borosilicate glass window. Top-right panel: the used PMT  
 14 was R2059 that is a timing PMT with a quartz window. Bottom-left panel: the used PMT was R6233-100sel that is a spectroscopic  
 15 PMT with a borosilicate glass window. Bottom-right panel: the used PMT was R6231-100mod that is a spectroscopic PMT with a  
 16 quartz window. The two windows W1 and W2, used for the PSD ratio, are indicated with black and grey dashed boxes, respectively

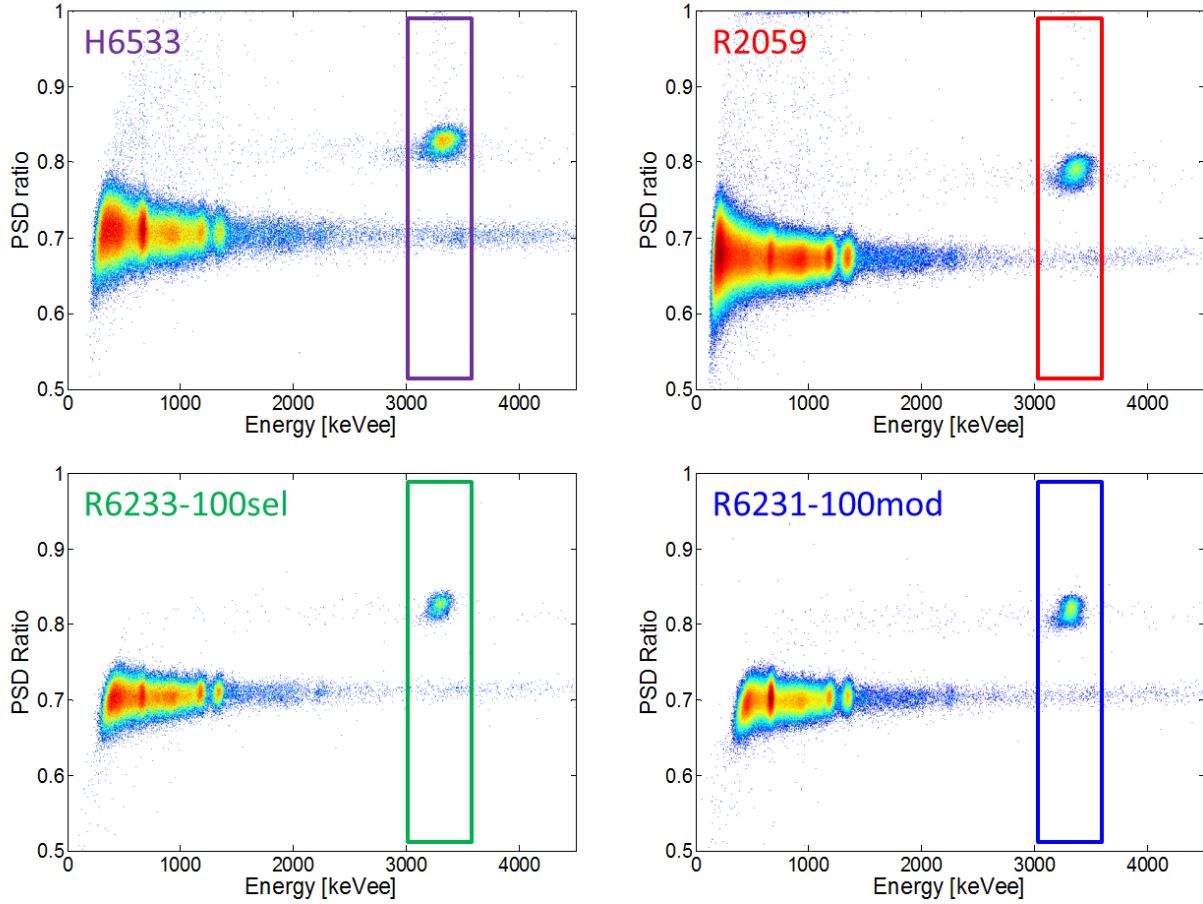
17

18 After the integration of the pulses within the two different time windows W1 and W2, we can define the PSD Ratio  
 19 as

$$PSD\ Ratio = \frac{W_2}{W_1 + W_2}$$

20  
21

22 Since the ratio between the W1 and W2 integrals is different for events relative to  $\gamma$  rays and neutrons, the PSD  
 23 Ratio allows us to discriminate between  $\gamma$  rays and neutrons event by event. The integral of the signal from the onset up  
 24 to 3  $\mu\text{s}$  is proportional to the total released energy (W3). By plotting the events in a matrix (PSD matrix) where the y  
 25 axis is the PSD Ratio and the x axis is W3 (i.e. the total energy), the neutron events appear clearly separated from the  
 26  $\gamma$ -ray ones, as can be seen in figure 4.



1  
2 **Figure 4:** The PSD matrices for the four different PMTs of table 1. Top-left panel: the used PMT was H6533 and a FOM of 2.8 was  
3 found (see text). Top-left right: the used PMT was R2059 and a FOM of 2.9 was found. Bottom-left panel: the used PMT was R6233-  
4 100sel and a FOM of 3.4 was found. Bottom-right panel: the used PMT was R6231-100mod and a FOM of 3.2 was found.

5  
6 Selecting the PSD matrix events in the rectangular box of figure 4 and projecting them on the y axis, we obtain a  
7 spectrum with two well separated peaks, one related to neutron events the other to  $\gamma$ -ray events. From the projection it is  
8 possible to extract a figure of merit (FOM), defined as:

$$9 \quad FOM = \frac{x_{cn} - x_{cy}}{FWHM_n + FWHM_\gamma},$$

10 where  $x_{cn}$  and  $x_{cy}$  are the centroids of the neutron and  $\gamma$ -ray peaks, while  $FWHM_n$  and  $FWHM_\gamma$  are the FWHMs of the  
11 neutron and  $\gamma$ -ray peaks, respectively. The FOM measures the capability of neutron- $\gamma$  discrimination.

12 The comparison between the four PMT's was performed in the same conditions: the same windows were chosen and no  
13 filter was applied. The resulting FOM values are 2.8, 2.9, 3.4 and 3.2 for H6533, R2059, R6233-100sel and R6231-  
14 100mod, respectively, with an estimated standard deviation of 0.1. Note that a FOM value of 1.5 provides a rejection  
15 ratio better than  $10^6$  (in the case of ideal Gaussian shapes of the projected peaks) [28]. It is important to point out that  
16 the typical rejection ratio of  $^3\text{He}$  detector is of the order of  $10^6$  [10]. From this comparison, we see that all tested PMTs  
17 give a good neutron- $\gamma$  discrimination. The obtained FOM values show that the effect of quartz or borosilicate windows  
18 is too small to be observed, which might not be surprising since only about 35% of the CVL light is filtered by the  
19 borosilicate window. We also note that the spectroscopic PMT's give a slightly better FOM than the others PMTs. This  
20 is somehow unexpected as, due to the fast rise-time of a timing PMT, one might hope that the timing PMT's produce a  
21 better discrimination between neutrons and  $\gamma$  events which might compensate for the worse energy resolution. Since the  
22 major difference between the timing and spectroscopic signals is in the first 10 ns, we also tried to reduce the time  
23 window length, considering the maximum in the first 5 ns (M1) and the integral of a 5 ns window at 300 ns after the  
24 signal onset (M2). The ratio M1/M2 between neutrons and  $\gamma$ -rays averaged pulses is much higher for timing PMTs than  
25 for the others. However, on an event by event basis, we found that, for timing PMTs, the FOM value (see equation 1)  
26 reduces to  $\sim 2$ , due to the fact that the pulse shape is less defined than in spectroscopic PMT's. The fact that the

spectroscopic PMTs produce a better FOM may be ascribed to the longer intrinsic rise time than the timing PMTs (see table 1). This, acting as a low pass filter, reduces the high frequency noise.

Even though one could use/define more complicated and "ad hoc" algorithms which take advantage on the  $\gamma$ -rays induced fast rising signal, we conclude that, using a simple algorithm, spectroscopic PMT's give a better neutron- $\gamma$  discrimination compared to timing PMT's. In addition, the energy resolution at 662 keV, measured from the W3 values, produced the values: 5 % for both the spectroscopic R6233-100sel and R6231-100mod PMTs, 7.2% for H6533 and 6.6% for R2059 PMTs.

As we have noticed that the removal of very high frequency noise might improve the FOM, we have also filtered the signals produced by the R6231-100mod PMT coupled to CLYC-6. In particular, a signal smoothing was applied (low pass filter) to improve the signal to noise ratio. Moreover a window W1 of 70 ns was used and a 100 MHz filter was applied to optimize the FOM value. The PSD ratio vs  $\gamma$ -rays energy matrix and its projection are shown in the left panel of figure 5. The two peaks corresponding to neutron and  $\gamma$ -ray events are shown in the right panel of figure 5. In this case it was possible to obtain a FOM value of 3.8.

FOM values, ranging from 1 to 4.8 are reported in Ref. [14, 26, 27]. They are from different CLYC samples, calculated in different energy ranges. The FOM values found in this work (from 2.8 to 3.8) agree with the reported values. It is important to point out that the FOM value depends on several parameters like the energy range of the neutrons, the count rate, the used algorithm, the filters applied on signals and so on. The highest FOM value found in literature, 4.8, [14], was found after an optimization of the pulse shape algorithms.

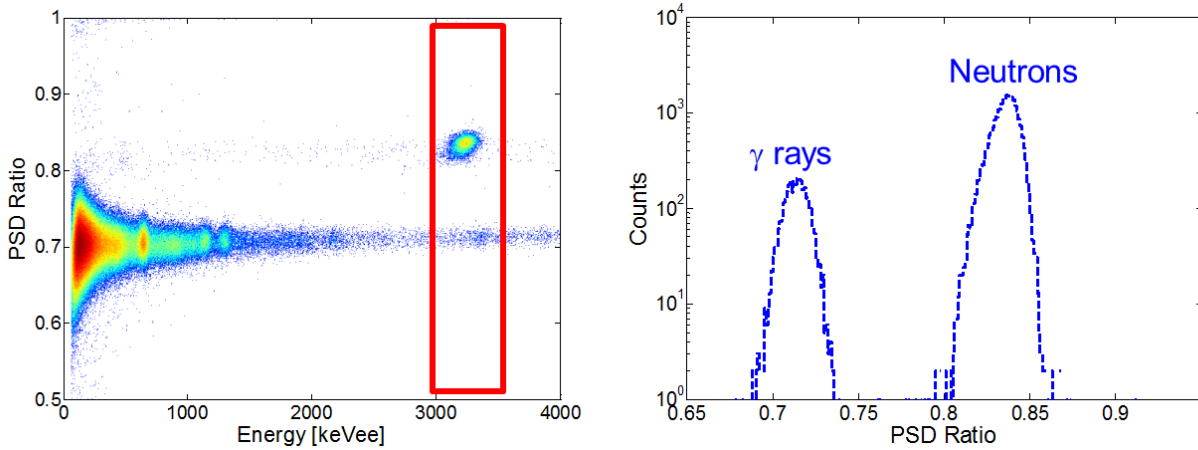


Figure 5: (Color on line) Left panel: the PSD matrix of CLYC-6 obtained using the HAMAMATSU R6231-100mod PMT and a digital filter (see text). In the matrix plot the z-axis is in logarithm scale. Right panel: The projection of the red box along the y axis of the PSD matrix. The measured FOM is 3.8.

PMT	$\gamma$ -ray rise time [ns]	$\gamma$ -ray fall time [ $\mu$ s]	neutron rise time [ns]	neutron fall time [ $\mu$ s]
H6533	2	0.8	30	1.8
R2059	3	0.9	33	1.8
R6233-100sel	17	1.0	40	1.7
R6231-100mod	14	1.0	37	1.7

Table 2: The rise time (10%-90% of full signal amplitude) and the fall time (90%-10% of full signal amplitude) of the  $\gamma$ -ray and neutron signals measured with the four PMTs of table 1.

### 3. Neutron identification

For the measurements of thermal and fast neutrons, the CLYC-6 and CLYC-7 scintillators were used. They were coupled to a HAMAMATSU R6231-100mod PMTs and to standard voltage dividers (HAMAMATSU E1198-26 and HAMAMATSU E1198-27 for CLYC-6 and CLYC-7, respectively). Data were taken with a 12 bit LeCroy Wave Runner oscilloscope (HDO ZI66).

#### 3.1 Thermal neutron detection

The thermal detection capability arises from  ${}^6\text{Li}$  ions, which have a 940 barns cross section for the reaction  ${}^6\text{Li}(n,\alpha){}^3\text{H}$ . Thermal neutrons were measured with both CLYC-6 and CLYC-7 crystals. The only difference between the two crystals is the Li isotope enrichment. In particular, as already mentioned, our CLYC-6 detector has an enrichment of 95% of  ${}^6\text{Li}$ , while the CLYC-7 crystal has an enrichment of  ${}^7\text{Li}$  higher than 99%, and is expected to be insensitive to thermal neutrons. In figure 6 the comparison between the energy spectra measured with the CLYC-6 (blue line) and the CLYC-7 (red line) detectors is shown. Both detectors were placed over a 40 cm box of polyethylene with a source of AmBe in the centre. The spectra of figure 6 are normalized on the  ${}^{137}\text{Cs}$  peak. The 3.2 MeV electron equivalent peak, induced by thermal neutrons, clearly visible in CLYC-6 spectrum, is absent in the CLYC-7 one. The FWHM of the thermal-neutron peak is 3.2 % for the CLYC-6 sample. The PSD matrix confirms the different sensitivity to thermal neutrons of CLYC-6 and CLYC-7, as shown in figure 7. The spot produced by thermal neutrons, which is present only in the CLYC-6 matrix, is clearly visible at PSD  $\sim 0.8$  and  $E = 3.2$  MeVee. The sensitivity ratio, calculated as the ratio between the events present in CLYC-6 and in CLYC-7 matrix in the region  $3.0 < x < 3.5$  MeV and  $0.76 < y < 0.81$ , is  $391 \pm 78$ . Consequently, we can conclude that the CLYC-7 detector has an efficiency to thermal neutrons less than  $\sim 0.3\%$  with respect to the CLYC-6 one. Assuming that the thermal neutron sensitivity comes only from  ${}^6\text{Li}$  nuclei we can extract a  ${}^6\text{Li}$  concentration in CLYC-7 crystal of  $0.26 \pm 0.05$  %. This value is consistent with what declared in the reference sheet by RMD.

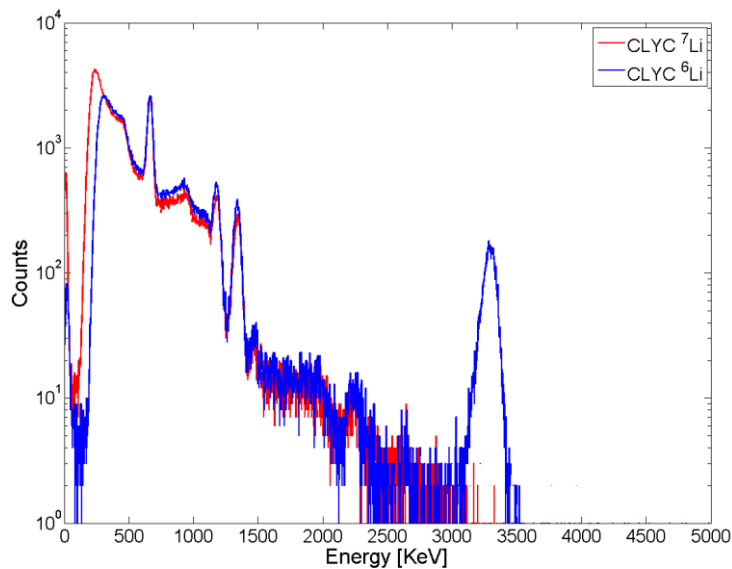
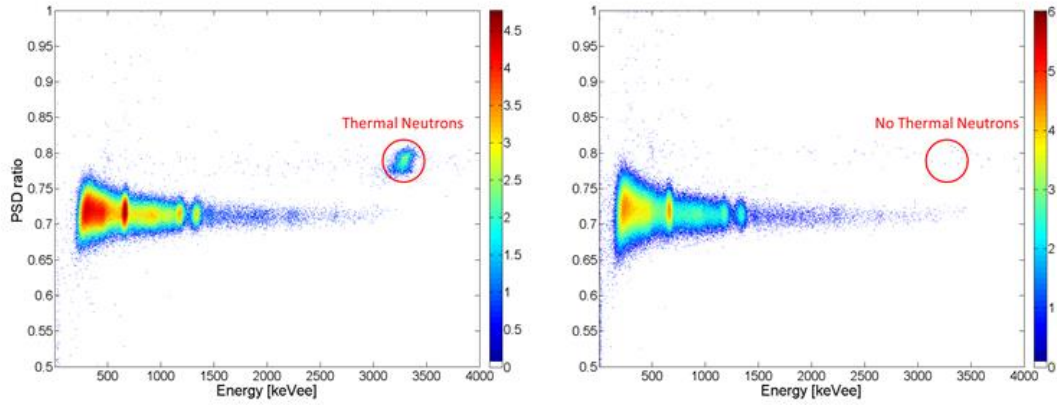


Figure 6: (Color on line) Spectra measured with a CLYC-6 and CLYC-7 placed near AmBe source in a paraffin box with side of 40 cm. The spectra were taken sequentially. The sources and the crystals were in the same position for both measurements. Both crystals were coupled to a R6231-100mod PMT, E1198-26 and E1198-27 VD for CLYC-6 and CLYC-7 respectively and powered at 1000 V. The energy thresholds in the two spectra were slightly different.





1  
2 *Figure 7: (Color on line) The PSD vs Energy 2D matrices of CLYC-6 (left panel) and CLYC-7 (right panel). The z-axis is in*  
3 *logarithm scale. The plots shows the capability to identify neutrons and  $\gamma$  rays in a CLYC scintillator. In the x axis there is the*  
4 *measured energy (electron equivalent) while in the y axis there is the PSD ratio (see text). The circle indicates thermal neutrons.*

### 5 **3.2 Fast neutron detection**

6 Fast neutrons are detected exploiting the reactions  $^{35}\text{Cl}(n, p)^{35}\text{S}$  and  $^{35}\text{Cl}(n, \alpha)^{32}\text{P}$ . The energy of the outgoing proton  
7 or  $\alpha$  particle is linearly related to the neutron energy. For this reason, CLYC scintillators are neutron spectrometers.  
8 Furthermore, the neutron kinetic energy can also be measured via the Time of Flight technique (FWHM < 1 ns) [14].  
9 A measurement was performed at the Neutron Generator at ENEA laboratories in Frascati (Italy), which provided 14.1  
10 MeV and  $\approx 2.5$  MeV neutrons.

11 The 14.1 MeV neutron emission was obtained by bombarding a tritium doped titanium target with a 300 keV  
12 deuterium beam [29]. The two samples of CLYC scintillators were placed at 1.25 m from the neutron source, as the flux  
13 was very high. The neutron generator of ENEA produced a neutron yield of  $5 \cdot 10^8$  n/s. It was measured by the standard  
14 neutron counting diagnostic, which consists of an absolutely calibrated detector measuring alpha particles produced by  
15 deuterium–tritium reactions in the target. We use the same set up and the same beam of ref. [7]. The neutron generator  
16 is at 4.5 m from the floor and walls, to reduce the thermal neutron background. Both CLYC detectors were used for the  
17 measurement of 14.1 MeV neutrons.

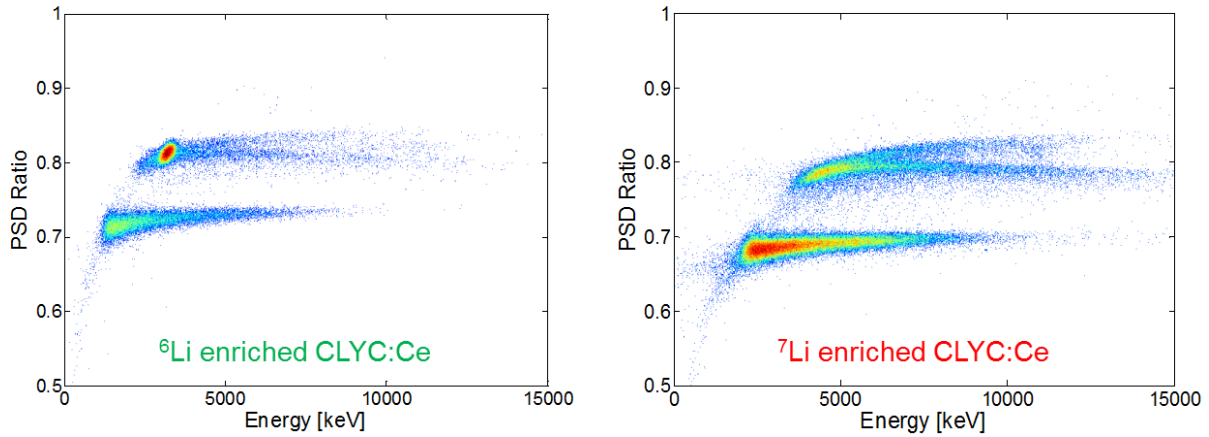
18 The left and right panels of figure 8 show the PSD matrices obtained with 14.1 MeV neutrons measured in CLYC-6  
19 and in CLYC-7 respectively. In both cases, the discrimination between  $\gamma$  rays and neutrons is clearly visible. The  
20 thermal neutron peak is present only in the left panel of figure 8 at about 3.2 MeVee. In the figure, the neutron events  
21 show two components probably due to protons and  $\alpha$  particles produced by the two reactions on  $^{35}\text{Cl}$  as suggested in ref  
22 [15]. In this case the neutron contribution appears as a continuum without any distinct peak. This feature may be  
23 connected to both the different two-three-body reactions that may occur with neutrons of 14.1 and the fact that the final  
24 nucleus might also be left in an excited state. At this energy, several three-body channels are open with a cross section  
25 even 10 times larger than the neutron capture on  $^{35}\text{Cl}$ . For example, the cross section of  $^{133}\text{Cs}(n, 2n)^{132}\text{Cs}$  is  $\sim 1.5$  barns  
26 whereas the cross sections of  $^{35}\text{Cl}(n, p)^{35}\text{S}$  and  $^{35}\text{Cl}(n, \alpha)^{32}\text{P}$  at 14.1 MeV is  $\sim 0.15$  barns only [22,24].

27 The continuum spectrum for neutrons with energy larger than 8 MeV was already observed by N. D'Olympia et al.  
28 [15]. They performed a simulation including all possible reactions on  $^{35}\text{Cl}$  and found that the major contribution is given  
29 by protons and  $\alpha$  particles, while no tritons or deuterons are expected to be produced by neutron induced reactions at  
30 these energies. The comparison between data and simulations was reasonably good, although the contributions of other  
31 neutron induced reactions cannot be excluded. A more detailed study of the emitted particles should be performed to  
32 understand which reactions are involved. The matrix shows also gamma events as in ref. [15,24]. These gamma rays  
33 could be due to background or prompt and delayed decays of nuclear excited states populated in the neutron induced  
34 reactions.

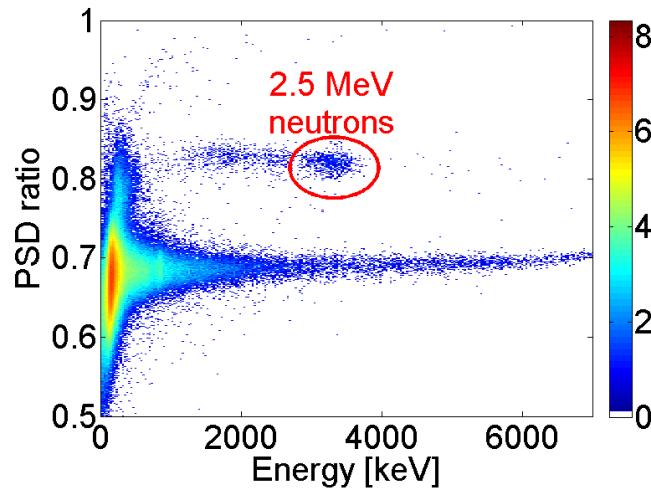
35 The 2.5 MeV neutrons were produced by the primary beam impinging on the beam dump, containing deuterium  
36 atoms. For this reason, the flux of the 2.5 MeV neutrons was weaker and less monochromatic than the flux of the 14.1  
37 MeV neutrons. In this case the energy of the thermal peak is expected to overlap with the proton energy produced by

1 the  $^{35}\text{Cl}(n,p)^{35}\text{S}$  reaction, because of the Q-value of the reaction, 0.6 MeV, to be added to the neutron energy. Since the  
 2 CLYC-7 crystal is almost not sensitive to thermal neutrons, as discussed in section 3.1, the 2.5 MeV neutrons were  
 3 detected using only this crystal. At this incident energy, the reaction  $^{35}\text{Cl}(n, \alpha)^{32}\text{P}$  is expected to have an almost  
 4 negligible cross section to be observed [22-24]. Figure 9 shows the resulting PSD matrix. The counts in the red circle,  
 5 where the neutron events are expected, are  $\sim 700$ . A comparison with the CLYC-6 detector taking into account the 0.3%  
 6 efficiency factor discussed in section 3.1 make us to estimate a maximum of  $\sim 13$  thermal neutron events in figure 9.

7 Previous measurements of monochromatic neutrons in this energy range are reported in ref. [15] and [24]. In  
 8 particular, in ref [24] a CLYC-6 crystal was used to detect 2.58 MeV neutrons, while 2.01 and 2.69 MeV neutrons were  
 9 detected by a CLYC-7 in ref [15]. Our results well compare with what found in both references, although in ref [24]  
 10 the presence of the thermal neutron peak partly overlaps with the fast neutron peak.  
 11 In our case, the FWHM of the proton peak is dominated by the spread in the incident neutron energy and cannot  
 12 therefore be compared with that observed in [15] and [24] where a monochromatic beam was used.



13  
 14 *Figure 8: (Color on line) The PDS matrixes obtained with fast neutrons of 14.1 MeV. Left panel: the matrix obtained with CLYC-6,*  
 15 *thermal neutron are evident as a spot located at  $x \sim 3200$  and  $y \sim 0.8$ . Right panel: the matrix obtained with CLYC-7. The z axis is in*  
 16 *log scale.*



17  
 18  
 19 *Figure 9: The PDS matrix obtained with fast neutron of 2.5 MeV measured with CLYC-7 scintillator. The neutron peak, related to*  
 20 *reaction  $^{35}\text{Cl}(n, p)^{35}\text{S}$  is indicated by the circle.*

21  
 22  
 23

## 5. Conclusions

In this work, we presented the results from the investigation of the performances of two 1"x1" samples of CLYC scintillators: one enriched with 95% of  $^6\text{Li}$  (CLYC-6) and the other with an enrichment of  $^7\text{Li}$  larger than 99% (CLYC-7). The CLYC scintillators exhibit good energy resolution under  $\gamma$ -ray excitation. We measured 4.8% and 4.5% at 662 keV for CLYC-6 and CLYC-7, respectively. An important property of these scintillators is the capability to identify and measure  $\gamma$  rays and neutrons via pulse shape discrimination. We have studied the signals produced by spectroscopic PMTs, by timing PMTs (which preserve the fast rise-time of the scintillation light) and quartz windows PMTs (which are sensitive to all the UV component). We have observed that the FOM for n- $\gamma$  discrimination, using the simple algorithm suggested in literature, is better for spectroscopic PMTs. The FOM value of 3.8 was found for thermal neutrons using a HAMAMATSU R6231-100mod PMT after filtering the signals. We also measured the CLYC internal radiation and we have found that it is at least two orders of magnitude smaller than that of an equivalent  $\text{LaBr}_3\text{:Ce}$  detector.

The thermal neutrons, produced by an AmBe source surrounded by polyethylene, were measured with both detectors. It was observed that the thermal neutron detection efficiency for the CLYC-7 is less than 0.3% with respect to the CLYC-6 sample. This value is consistent with what declared in the reference sheet of RMD (concentration of  $^6\text{Li} < 1\%$ ). In order to test the capability of these crystals to detect fast neutrons, an experiment was performed at the Frascati Neutron Generator facility (Italy). A deuterium beam was used to provide neutrons of  $\sim 2.5$  MeV or 14.1 MeV, respectively. We found a peak related to 2.5 MeV neutrons and a continuum energy spectrum for 14.1 MeV neutrons, due to a superimposition of different reaction mechanisms.

### ACKNOWLEDGMENTS

The project is co-financed by the European Union and the European Social Fund. This work was also supported by *NuPNET - ERA-NET* within the the NuPNET GANAS project, under grant agreement n° 202914 and from the European Union, within the "7<sup>th</sup> Framework Program" FP7/2007-2013, under grant agreement n° 262010 – ENSAR-INDESYS. This work was also supported by "Programmi di Ricerca Scientifica di Rilevante Interesse Nazionale" (PRIN) number2001024324\_01302.

### References

- [1] A.Giaz et al in print on Nuclear Instruments and Methods A
- [2] "BrillLanCe Scintillators Performance Summary.pdf" available at <http://www.detectors.saint-gobain.com/Brilliance380.aspx>.
- [3] O. Guillot-Noël, (1999) et al., J. Lumin., 85, 21.
- [4] E. V. D. Van Loef, (2001), et al., Appl. Phys. Lett., 79, 1574.
- [5] R.Nicolini et al. Nucl. Inst. and Meth. A 582 (2007) 554-561.
- [6] A. Giaz et al., Nucl. Inst. and Meth. A 729 (2013) 910–921.
- [7] C.Cazzaniga et al. Nucl. Instrum. Meth. A 778 (2015) 20.
- [8] M.Ciemala et al. Nucl. Instrum. Meth. A608(2009)76 .
- [9] J. Glodo et al., IEEE TNS 55 (2008)1206 and IEEE TNS 56(2009)1257
- [10] J. Glodo et al., IEEE TNS, 58 (2011)333.
- [11] J. Glodo et al., Journal of Crystal Growth 79(2013)73
- [12] B.S. Budden et al. IEEE TNS, 60(2013)946.
- [13] M.B.Smith at al. Nucl. Instr. and Meth. A784(2015)162.
- [14] N.D'Olympia et al. Nucl. Instr. and Meth. A714(2013)121.
- [15] N.D'Olympia et al. Nucl. Instr. and Meth. A763(2014)433.
- [16] K.Yang and P.Menge Nucl. Instr. and Meth. A784(2015)74.

- 1 [17] R. Machrafi et al. Radiation Measurements 70(2014)5.
- 2 [18] N. Cherepy et al. , IEEE TNS, 60 (2013) 955.
- 3 [19] F. Quarati, et al., Nucl. Instr. and Meth. A 729 (2013) 596.
- 4 [20] R. Billnert et al. Nucl. Instr. and Meth. A 647 (2011)94.
- 5 [21] N. Cherepy et al. Nucl. Sci. Symp. and Med. Im. Conf. (NSS/MIC), (2012) 1692-1697.
- 6 [22] Pointwise ENDF-VII library at 300 K: <http://atom.kaeri.re.kr>
- 7 [23] D'Olympia et al. Nucl. Instr. and Meth. A694(2012)140.
- 8 [24] M.B. Smith et al. IEEE TNS, 60(2013)855.
- 9 [25] RMD - <http://rmdinc.com/clyc/>
- 10 [26] D.W. Lee et al., Nucl. Instr. and Meth, A664, (2012),1 and references therein.
- 11 [27] M. Martone, M. Angelone, M. Pillon., Journal of Nuclear Materials 212 (1994) 1661.
- 12 [28] A. Winyard et al. NUcl. Instr. and Meth. A95(1971)141
- 13 [29] [www.fusione.enea.it/LABORATORIES/Tec/FNG.html](http://www.fusione.enea.it/LABORATORIES/Tec/FNG.html).it